

A Moment–Hankel Rank Method for Identifying the Number of Point Sources in the Heat Equation

Zhiliang Deng¹ , Xiaomei Yang^{2,*} and Ailin Qian³

¹School of Mathematical Science, University of Electronic Science and Technology of China, Chengdu, China

²School of Mathematics, Southwest Jiaotong University, Chengdu, China

³Department of Mathematics and Statistics, Hubei University of Science and Technology, Xianning, Hubei

E-mail: yangxiaomaht@swjtu.edu.cn

Keywords: inverse heat source problem, point source, source counting, boundary flux data, Fourier moments, Hankel matrix, numerical rank, singular-value stability

Abstract

We develop a low-frequency moment–Hankel rank method for identifying the number of time-independent point sources in the heat equation from boundary flux data. The method is formulated in the unit disk, where the Laplace-transformed and normalized boundary flux admits an explicit Fourier moment representation. By taking the low-frequency limit, we obtain a finite exponential-sum moment sequence in which the nodes encode the source locations, the weights encode the source strengths, and the number of terms equals the number of point sources. The associated Hankel matrix admits a Vandermonde factorization, and its rank is exactly the source number under the natural assumptions that the source locations are distinct and the source strengths are nonzero. We also analyze the effect of discrete and noisy boundary data. A uniform moment perturbation bound is propagated to the empirical Hankel matrix, and Weyl’s singular-value perturbation inequality yields a sufficient condition for stable numerical rank recovery in terms of the smallest nonzero singular value of the ideal Hankel matrix. Numerical experiments confirm the exact rank pattern in the noiseless case, validate the stability threshold under moment noise, and illustrate the loss of resolution for close or weak sources. After the source number is identified, the same moment sequence can be used for location and strength recovery through an annihilating-polynomial and Vandermonde reconstruction procedure.

1 Introduction

In this paper, we consider a point source recovery problem governed by the heat equation in the unit disk $\mathbb{D} \subset \mathbb{R}^2$

$$\begin{cases} \partial_t u(x, t) - \Delta u(x, t) = \sum_{j=1}^N q_j \delta(x - p_j), & (x, t) \in \mathbb{D} \times (0, \infty), \\ u(x, t) = 0, & (x, t) \in \partial\mathbb{D} \times (0, \infty), \\ u(x, 0) = 0, & x \in \mathbb{D}. \end{cases} \quad (1.1)$$

where the locations $p_j \in \mathbb{D}$, the strengths $q_j \neq 0$, and the number N of sources are unknown and need to be determined from the boundary heat fluxes

$$f(\theta, t) = \frac{\partial u}{\partial \nu}(e^{i\theta}, t), \quad 0 \leq \theta < 2\pi. \quad (1.2)$$

Inverse source problems for parabolic equations have received considerable attention over the past decades. Classical results on uniqueness, stability, and reconstruction have been established for a range of settings, including different observation types, source regularities, and a priori information [5, 6, 7, 14, 15, 16, 23, 25, 27]. These developments have been largely driven by applications such as medical imaging, environmental monitoring, groundwater contamination identification, and structural health monitoring [2, 3, 4, 10, 13, 18, 21, 26]. Nevertheless, the recovery of point sources represented by Dirac measures remains a distinct inverse problem, because the unknown source configuration contains not only locations and strengths, but also the number of active sources.

For heat equations with point sources, several recent works are directly related to the present study. Ling et al. [19] showed, under the assumption that the source function is a sum of known spatial functions, that one measurement point can identify the number of sources and three measurement points can determine all source locations in two-dimensional domains. Gong et al. [11] proved uniqueness for recovering one point source with a piecewise constant-in-time amplitude from boundary flux data, using eigenfunction expansions, kernel estimates, and complex-analytic arguments. Gu et al. [12] established a uniqueness theorem for a Dirac point source from sparse boundary measurements and proposed a least-squares reconstruction method solved by gradient descent. Deng et al. [9] developed a Bayesian thinning algorithm to infer the number, locations, and intensities of heat point sources when the cardinality is unknown. In [8], Deng et al. introduced a Hankel determinant characteristic for determining the number of point sources and used the argument principle to compute the associated determinant zero count.

Algebraic Hankel-type methods have also appeared in related inverse source problems for elliptic equations. Abdelaziz et al. [1] studied inverse source problems for two-dimensional elliptic equations, including the Helmholtz equation, from Cauchy data. They considered pointwise sources and sources supported in small subdomains, derived reciprocity-gap type algebraic identities, and constructed Hankel-type matrices to recover source information through rank identification and a companion-matrix procedure. Point-source recovery problems for other types of equations have also been studied; see, for example, [4, 17, 20, 22, 24, 28]. These works show that point-source identification often admits finite-dimensional algebraic structures, but the precise structure depends strongly on the governing equation and on the type of boundary data.

The present paper follows a different low-frequency moment route for stationary point sources in the heat equation. After Laplace transformation and normalization, we take the low-frequency limit of the boundary heat flux and compute its positive Fourier moments. These moments form a finite exponential-sum sequence: the nodes encode the source locations, the weights encode the source strengths, and the number of exponential terms is the number of point sources. The associated Hankel matrix admits a Vandermonde factorization, and its rank equals the source number when the source locations are distinct and the strengths are nonzero.

This rank-based mechanism is different from the determinant zero-counting approach in [8]. There the source number is encoded in the zero order of an analytic Hankel determinant characteristic $\Delta_m(s)$, and the computation is implemented by an argument-principle contour integral in the complex Laplace-frequency plane. Here we use only the low-frequency moment sequence and obtain a static Hankel matrix. Therefore the source number is identified from the rank, or numerical rank, of this matrix. For discrete and noisy boundary data, we further quantify the perturbation of the singular values by Weyl's inequality and derive a sufficient condition for stable numerical source counting. Once the source number is determined, the same moment sequence can be used to recover source locations and strengths through an annihilating-polynomial and Vandermonde reconstruction procedure.

The rest of the paper is organized as follows. The remainder of the Introduction formulates the inverse heat point-source problem and introduces the normalized boundary flux. Section 2 derives the low-frequency moment representation and proves the moment–Hankel rank characterization of the source number. Section 3 discusses discrete boundary measurements, noisy moments, and numerical rank selection. Section 4 presents numerical experiments, and Section 5 concludes the paper.

2 Moment–Hankel Rank Principle

This section derives the moment–Hankel rank principle for source counting. Starting from the Laplace-transformed boundary flux, we first remove the known factor caused by the time-independent source strength and introduce the normalized boundary flux. We then take its low-frequency limit and show that the resulting positive Fourier moments form a finite exponential sum. This finite-dimensional structure yields a Hankel matrix with a Vandermonde factorization. As a consequence, the rank of the Hankel matrix equals the number of point sources under the natural assumptions that the source locations are distinct and the source strengths are nonzero.

The Laplace transform (with respect to t) of system (1.1), using the initial condition $u(x, 0) = 0$, yields the following boundary value problem for the modified Helmholtz equation:

$$\begin{cases} s\hat{u}(x, s) - \Delta\hat{u}(x, s) = \frac{1}{s} \sum_{j=1}^N q_j \delta(x - p_j), \\ \hat{u}|_{\partial\mathbb{D}} = 0. \end{cases} \quad (2.1)$$

Let $G_s(x, y)$ denote the Green's function for the modified Helmholtz operator $s - \Delta$ on \mathbb{D} with homogeneous Dirichlet boundary conditions. Then the solution \widehat{u} can be expressed as

$$\widehat{u}(x, s) = \frac{1}{s} \sum_{j=1}^N q_j G_s(e^{i\theta}, p_j). \quad (2.2)$$

Therefore the Laplace transform of the boundary flux takes the form

$$\widehat{f}(\theta, s) = \frac{1}{s} \sum_{j=1}^N q_j \frac{\partial G_s}{\partial \nu_z}(e^{i\theta}, p_j). \quad (2.3)$$

Since the factor $1/s$ is known, we use the normalized boundary flux

$$\mathcal{F}(\theta, s) := s\widehat{f}(\theta, s). \quad (2.4)$$

The proposed source-counting method is based on the low-frequency limit of $\mathcal{F}(\theta, s)$.

Let

$$g(\theta) := \lim_{s \rightarrow 0} \mathcal{F}(\theta, s). \quad (2.5)$$

Since $G_s \rightarrow G_0$ as $s \rightarrow 0$, where G_0 is the Dirichlet Green function for $-\Delta$ in the unit disk, we have

$$g(\theta) = \sum_{j=1}^N q_j \frac{\partial G_0}{\partial \nu_z}(e^{i\theta}, p_j). \quad (2.6)$$

Writing $p_j = \rho_j e^{i\phi_j}$, $0 \leq \rho_j < 1$, the boundary normal derivative of G_0 admits the Fourier expansion

$$\frac{\partial G_0}{\partial \nu_z}(e^{i\theta}, p_j) = -\frac{1}{2\pi} \sum_{n=-\infty}^{\infty} \rho_j^{|n|} e^{in(\theta - \phi_j)}. \quad (2.7)$$

Define the positive Fourier moments

$$\mathcal{M}_n = \frac{1}{2\pi} \int_0^{2\pi} g(\theta) e^{-in\theta} d\theta, \quad n = 0, 1, \dots \quad (2.8)$$

According to (2.6) and (2.7), we have the representation

$$\mathcal{M}_n = -\frac{1}{2\pi} \sum_{j=1}^N q_j (\rho_j e^{-i\phi_j})^n. \quad (2.9)$$

With

$$\lambda_j := \rho_j e^{-i\phi_j}, \quad w_j := -\frac{q_j}{2\pi},$$

the moments take the finite exponential-sum form

$$\mathcal{M}_n = \sum_{j=1}^N w_j \lambda_j^n, \quad n = 0, 1, \dots \quad (2.10)$$

Thus the source configuration is encoded in the moment sequence $\{\mathcal{M}_n\}_{n \geq 0}$: the nodes λ_j , the weights w_j , and the number of exponential terms correspond respectively to the source locations, strengths, and source number.

To extract the number of exponential terms from the moment sequence, we define, for $m \geq 1$, the Hankel matrix

$$H_m = (\mathcal{M}_{r+c})_{r,c=0}^{m-1}. \quad (2.11)$$

Using the finite exponential-sum representation (2.10), we obtain the factorization

$$H_m = V_m(\lambda) \text{diag}(w_1, \dots, w_N) V_m(\lambda)^\top, \quad (2.12)$$

where

$$V_m(\lambda) = (\lambda_j^r)_{r=0, \dots, m-1; j=1, \dots, N}. \quad (2.13)$$

Theorem 2.1. Assume that the source locations are distinct and that the source strengths are nonzero. Equivalently,

$$\lambda_i \neq \lambda_j \quad (i \neq j), \quad w_j \neq 0.$$

Then, for every $m \geq N$,

$$\text{rank } H_m = N.$$

Consequently, if m is chosen no smaller than the true source number, then the number of point sources is determined by the rank of the Hankel matrix.

Proof. Since the nodes $\lambda_1, \dots, \lambda_N$ are pairwise distinct, $V_m(\lambda)$ has full column rank for $m \geq N$. Since all weights are nonzero, $\text{diag}(w_1, \dots, w_N)$ is nonsingular. Therefore the factorization of H_m gives $\text{rank } H_m = N$. \square

Remark 2.2. Theorem 2.1 is the algebraic basis of the proposed source-counting method. It shows that the low-frequency boundary moments convert the inverse point-source counting problem into a finite-dimensional rank-identification problem. In contrast to complex-frequency determinant methods, no contour integral or zero-order computation is needed at this stage: the number of sources is read directly from the rank of a static Hankel matrix.

In exact data, this gives $N = \text{rank } H_m$ for any $m \geq N$. For discrete and noisy data, the exact rank is replaced by a numerical rank computed from the singular values of the empirical Hankel matrix. The method is therefore stable when the N -th singular value is well separated from the noise floor, which in turn requires sufficiently separated source nodes and non-negligible source strengths.

3 Discrete Data and Numerical Rank Selection

This section turns the exact rank characterization into a practical source-counting procedure from discrete and noisy boundary data. In computations, the low-frequency boundary data $g(\theta)$ are available only at finitely many boundary points and are usually contaminated by measurement noise. We first approximate the Fourier moments by a discrete quadrature and form an empirical Hankel matrix. We then estimate how boundary sampling and measurement noise perturb the moments. Finally, using Weyl's inequality for singular values, we derive a sufficient condition under which the numerical rank of the perturbed Hankel matrix still gives the true source number.

3.1 Discrete and noisy moments

Suppose that the boundary is sampled at uniformly distributed points

$$\theta_\ell = \frac{2\pi(\ell-1)}{L}, \quad \ell = 1, \dots, L.$$

The positive Fourier moments are approximated by the trapezoidal rule

$$\mathcal{M}_n^{(L)} = \frac{1}{L} \sum_{\ell=1}^L g(\theta_\ell) e^{-in\theta_\ell}, \quad n = 0, 1, \dots, 2m-2. \quad (3.1)$$

The corresponding discrete Hankel matrix is

$$H_m^{(L)} = \left(\mathcal{M}_{r+c}^{(L)} \right)_{r,c=0}^{m-1}. \quad (3.2)$$

In the presence of noisy boundary data, let

$$g_\ell^\delta = g(\theta_\ell) + \eta_\ell, \quad \ell = 1, \dots, L, \quad (3.3)$$

where η_ℓ denotes the measurement noise at the boundary point θ_ℓ . The noisy discrete moments are

$$\tilde{\mathcal{M}}_n = \frac{1}{L} \sum_{\ell=1}^L g_\ell^\delta e^{-in\theta_\ell}, \quad n = 0, 1, \dots, 2m-2, \quad (3.4)$$

and the corresponding empirical Hankel matrix is

$$\tilde{H}_m = \left(\tilde{\mathcal{M}}_{r+c} \right)_{r,c=0}^{m-1}. \quad (3.5)$$

The exact rank identity in Theorem 2.1 no longer applies directly to \tilde{H}_m , because noise and quadrature errors lift the zero singular values of the ideal Hankel matrix. Therefore the exact rank must be replaced by a numerical rank determined from the singular-value spectrum.

3.2 A bound for the moment error

We first relate the perturbation of the moment sequence to boundary noise and discrete sampling. Write

$$\widetilde{\mathcal{M}}_n = \mathcal{M}_n + e_n, \quad n = 0, 1, \dots, 2m - 2.$$

We shall use the aggregate moment error

$$\max_{0 \leq n \leq 2m-2} |e_n| \leq \varepsilon_m. \quad (3.6)$$

Assume first that the boundary noise satisfies the deterministic bound

$$|\eta_\ell| \leq \delta_g, \quad \ell = 1, \dots, L.$$

Then the noise contribution to the moment perturbation is bounded by

$$\left| \frac{1}{L} \sum_{\ell=1}^L \eta_\ell e^{-in\theta_\ell} \right| \leq \delta_g, \quad n = 0, 1, \dots, 2m - 2. \quad (3.7)$$

There is also a deterministic quadrature error. Since all sources lie strictly inside the unit disk, the Fourier coefficients of g decay geometrically. Indeed, by (2.6) and (2.7), we have

$$g(\theta) = -\frac{1}{2\pi} \sum_{j=1}^N q_j \sum_{k \in \mathbb{Z}} \rho_j^{|k|} e^{ik(\theta - \phi_j)}.$$

Denoting $c_k := -\frac{1}{2\pi} \sum_{j=1}^N q_j \rho_j^{|k|} e^{-ik\phi_j}$, we have

$$g(\theta) = \sum_{k \in \mathbb{Z}} c_k e^{ik\theta}.$$

Let

$$\rho_* := \max_{1 \leq j \leq N} |\rho_j| < 1, \quad Q := \frac{1}{2\pi} \sum_{j=1}^N |q_j|.$$

It follows that

$$|c_k| \leq \frac{1}{2\pi} \sum_{j=1}^N |q_j| \rho_j^{|k|} \leq Q \rho_*^{|k|}, \quad k \in \mathbb{Z}.$$

For $L > 2m - 2$, the trapezoidal rule gives the aliasing relation

$$\mathcal{M}_n^{(L)} = \sum_{j \in \mathbb{Z}} c_{n+jL}, \quad 0 \leq n \leq 2m - 2.$$

Hence we get

$$\begin{aligned} \left| \mathcal{M}_n^{(L)} - \mathcal{M}_n \right| &\leq \sum_{j \neq 0} |c_{n+jL}| \leq \frac{Q(\rho_*^{L-n} + \rho_*^{L+n})}{1 - \rho_*^L} \\ &\leq \frac{2Q\rho_*^{L-(2m-2)}}{1 - \rho_*^L}, \quad 0 \leq n \leq 2m - 2. \end{aligned} \quad (3.8)$$

Consequently, the total moment error can be bounded by

$$\varepsilon_m \leq \delta_g + \frac{2Q\rho_*^{L-(2m-2)}}{1 - \rho_*^L}. \quad (3.9)$$

This estimate separates the measurement-noise contribution from the deterministic boundary-sampling error.

3.3 Stability of numerical rank selection

We now show how the moment perturbation affects the singular values of the Hankel matrix. Define

$$E_m := \tilde{H}_m - H_m = (e_{r+c})_{r,c=0}^{m-1}.$$

By (3.6), each entry of E_m is bounded by ε_m . Hence, with $\|\cdot\|_2$ denoting the spectral norm and $\|\cdot\|_F$ denoting the Frobenius norm, we have

$$\|E_m\|_2 \leq \|E_m\|_F = \left(\sum_{r,c=0}^{m-1} |e_{r+c}|^2 \right)^{1/2} \leq m\varepsilon_m. \quad (3.10)$$

Lemma 3.1. *Let*

$$\sigma_1(H_m) \geq \sigma_2(H_m) \geq \cdots \geq \sigma_m(H_m) \geq 0$$

and

$$\sigma_1(\tilde{H}_m) \geq \sigma_2(\tilde{H}_m) \geq \cdots \geq \sigma_m(\tilde{H}_m) \geq 0$$

be the singular values of H_m and \tilde{H}_m , respectively. If (3.6) holds, then

$$\left| \sigma_k(\tilde{H}_m) - \sigma_k(H_m) \right| \leq m\varepsilon_m, \quad k = 1, \dots, m. \quad (3.11)$$

Proof. By Weyl's perturbation inequality for singular values, we have

$$\left| \sigma_k(\tilde{H}_m) - \sigma_k(H_m) \right| \leq \|\tilde{H}_m - H_m\|_2 = \|E_m\|_2.$$

Combining this estimate with (3.10) gives (3.11). \square

The preceding lemma yields a sufficient condition for stable source counting. Let $m \geq N$. By Theorem 2.1,

$$\text{rank } H_m = N.$$

Therefore

$$\sigma_N(H_m) > 0, \quad \sigma_{N+1}(H_m) = \cdots = \sigma_m(H_m) = 0.$$

The quantity $\sigma_N(H_m)$ is the smallest signal singular value of the ideal Hankel matrix.

Theorem 3.2. *Assume that $m \geq N$, the source locations are distinct, and the source strengths are nonzero. Suppose that the moment perturbation satisfies (3.6) and*

$$m\varepsilon_m < \frac{1}{2}\sigma_N(H_m). \quad (3.12)$$

Let the numerical rank estimator be

$$\hat{N} = \#\{k : \sigma_k(\tilde{H}_m) > \tau_m\}, \quad (3.13)$$

where the threshold τ_m satisfies

$$m\varepsilon_m < \tau_m < \sigma_N(H_m) - m\varepsilon_m. \quad (3.14)$$

Then

$$\hat{N} = N. \quad (3.15)$$

Proof. For $k \leq N$, Lemma 3.1 gives

$$\sigma_k(\tilde{H}_m) \geq \sigma_k(H_m) - m\varepsilon_m \geq \sigma_N(H_m) - m\varepsilon_m > \tau_m.$$

For $k > N$, since $\sigma_k(H_m) = 0$, Lemma 3.1 gives

$$\sigma_k(\tilde{H}_m) \leq m\varepsilon_m < \tau_m.$$

Thus exactly the first N singular values of \tilde{H}_m exceed τ_m , which proves $\hat{N} = N$. \square

Remark 3.3. *Theorem 3.2 shows that the stability of the moment–Hankel rank method is governed by the gap between the smallest signal singular value $\sigma_N(H_m)$ and the zero singular values of the ideal Hankel matrix. Since $\sigma_{N+1}(H_m) = 0$, this gap is precisely $\sigma_N(H_m)$. Close source locations or very weak source strengths reduce $\sigma_N(H_m)$, and therefore reduce the admissible perturbation level. This explains why near-colliding sources and weak sources are more difficult to identify from noisy data.*

3.4 Practical rank estimators

Theorem 3.2 gives a sufficient condition for exact rank recovery. Its threshold condition is useful for analysis, but it cannot be applied directly in computation because it involves the unknown ideal quantity $\sigma_N(H_m)$ and the unknown source number N . We therefore use practical rank-selection rules based only on the singular values of the empirical Hankel matrix \tilde{H}_m .

Let

$$\sigma_1^\delta \geq \sigma_2^\delta \geq \dots \geq \sigma_m^\delta \geq 0$$

be the singular values of \tilde{H}_m . In the ideal case, exactly the first N singular values are nonzero, while the remaining singular values are zero. In noisy data, the zero singular values are lifted by perturbations. Thus the source-counting problem becomes the problem of separating significant singular values from the noise floor.

When an estimate of the relative moment noise level δ is available, we use the noise-aware threshold

$$\tau_\delta = c_{\text{noise}} \delta \sigma_1^\delta, \quad (3.16)$$

where $c_{\text{noise}} > 0$ is a safety factor and σ_1^δ gives the scale of the empirical Hankel matrix. The estimated source number is

$$\hat{N} = \#\{k : \sigma_k^\delta > \tau_\delta\}. \quad (3.17)$$

This rule counts the singular values that are significantly above the estimated noise level.

When the noise level is unavailable, one may instead use the largest relative gap in the singular-value sequence:

$$\hat{N} = \arg \max_{1 \leq k \leq m-1} \frac{\sigma_k^\delta}{\sigma_{k+1}^\delta}.$$

This heuristic is motivated by the ideal rank structure: the largest drop in the singular values is expected to occur between the last signal singular value σ_N^δ and the first noise-dominated singular value σ_{N+1}^δ .

The numerical experiments below compare these two practical rank-selection rules. Their performance is then interpreted using the stability ratio

$$\frac{m\varepsilon_m}{\sigma_N(H_m)},$$

which measures the perturbation level relative to the smallest ideal signal singular value.

4 Numerical Experiments

In this section, we test the proposed moment–Hankel rank method and examine its stability in connection with the singular-value perturbation result in Theorem 3.2. The purpose is to illustrate the low-frequency rank characterization established in Theorem 2.1 and to show how the smallest signal singular value controls the practical performance of numerical rank selection.

All experiments are carried out in the unit disk. The low-frequency moments are generated from the finite exponential-sum representation

$$\mathcal{M}_n = \sum_{j=1}^N w_j \lambda_j^n, \quad \lambda_j = \bar{p}_j, \quad w_j = -\frac{q_j}{2\pi},$$

derived in Section 2. Unless otherwise stated, the Hankel order is chosen as $m = 8$.

For noisy experiments, we perturb the moment sequence directly in order to isolate the stability of the moment–Hankel rank step. For a relative moment noise level δ , we use

$$\mathcal{M}_n^\delta = \mathcal{M}_n + \delta \left(\frac{1}{2m-1} \sum_{k=0}^{2m-2} |\mathcal{M}_k|^2 \right)^{1/2} \xi_n, \quad n = 0, 1, \dots, 2m-2,$$

where ξ_n are independent standard complex Gaussian random variables. The source number is estimated either by the noise-aware threshold rule

$$\hat{N} = \#\{k : \sigma_k^\delta > \tau_\delta\}, \quad \tau_\delta = c_{\text{noise}} \delta \sigma_1^\delta,$$

or by the largest-gap rule applied to the singular-value sequence of the noisy Hankel matrix. In the reported experiments, $c_{\text{noise}} = 5$, and each Monte Carlo success rate is computed from 200 independent noise realizations.

For each noisy trial, we also compute the observed moment perturbation

$$\varepsilon_m^{\text{obs}} = \max_{0 \leq n \leq 2m-2} |\mathcal{M}_n^\delta - \mathcal{M}_n|$$

and the stability ratio

$$R = \frac{m\varepsilon_m^{\text{obs}}}{\sigma_N(H_m)}.$$

According to Theorem 3.2, the condition

$$R < \frac{1}{2}$$

is sufficient for stable numerical rank recovery, provided that the rank threshold is chosen between the perturbation level and the smallest signal singular value.

4.1 Noiseless Hankel rank pattern

We first verify the rank characterization in the noiseless case. For $N = 1, \dots, 5$, we construct deterministic source configurations with distinct locations and nonzero strengths, compute the exact moment sequence, and form the Hankel matrices H_m for $m = 1, \dots, 9$.

Figure 1 shows the singular-value spectra of H_8 and the numerical rank as the Hankel order varies. The singular-value spectra display a sharp drop after the N -th singular value, while the remaining singular values are at the level of machine precision. The numerical rank pattern is exactly

$$\text{rank } H_m = \min\{m, N\},$$

and in particular

$$\text{rank } H_m = N \quad \text{for all } m \geq N.$$

This confirms the moment–Hankel rank principle in Theorem 2.1.

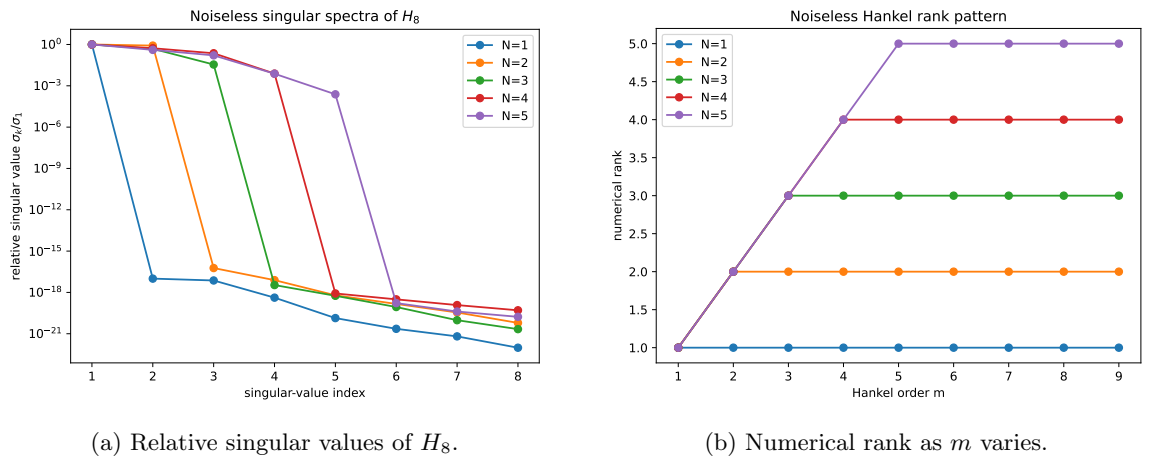


Figure 1: Noiseless moment–Hankel rank identification. The singular-value spectra show a clear drop after the N -th singular value, and the numerical rank satisfies $\text{rank } H_m = N$ once $m \geq N$.

4.2 Noise sensitivity and Weyl-type stability threshold

We next examine the effect of moment noise on numerical rank selection and compare the observed behavior with the Weyl-type stability condition in Theorem 3.2. For each $N = 1, \dots, 5$, the same source configurations as in the noiseless experiment are used. Independent complex Gaussian perturbations are added to the moments at the noise levels

$$\delta = 0, 10^{-5}, 10^{-4}, 10^{-3}, 10^{-2}, 3 \times 10^{-2}, 5 \times 10^{-2}.$$

Figure 2 compares the largest-gap rule and the noise-aware threshold rule. The threshold rule is more consistent with the singular-value perturbation analysis. For $N = 1$ and $N = 2$, it correctly identifies the source number for all tested noise levels. For $N = 3$ and $N = 4$, it remains accurate

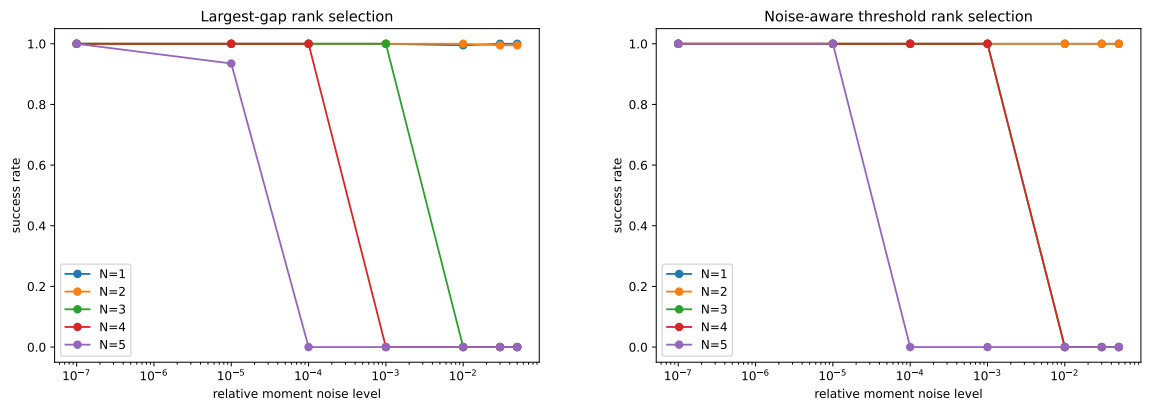
for small noise levels, but fails when the smallest signal singular values are absorbed into the noise floor. For $N = 5$, the rank estimate becomes sensitive much earlier. The largest-gap rule is useful as a heuristic when no noise level is available, but it becomes less stable for larger N , especially when noise lifts several small singular values.

The stability ratio shown in Figure 3 explains this transition. When the median value of

$$R = \frac{m\varepsilon_m^{\text{obs}}}{\sigma_N(H_m)}$$

stays below $1/2$, the threshold rank selector is reliable. Once this ratio crosses the sufficient threshold $1/2$, the success rate drops sharply. Thus the numerical transition from successful rank recovery to failure is consistent with the sufficient condition in Theorem 3.2. The condition is not necessary, but it provides a clear and computable diagnostic for when numerical rank selection can be trusted.

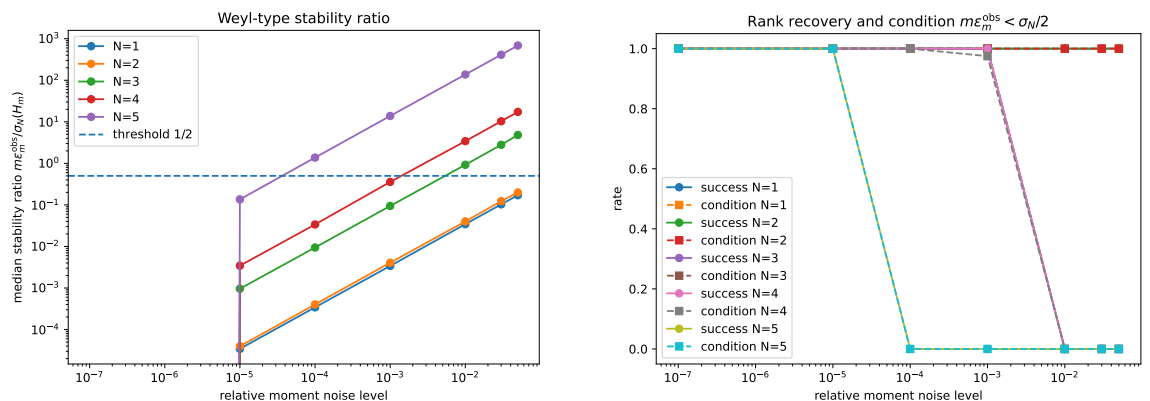
The dominant failure mode is underestimation of the source number. This is expected from the singular-value structure: noise lifts the zero singular values, while small nonzero signal singular values may be pushed below the chosen threshold. As a result, sources associated with weak singular directions are missed.



(a) Largest-gap rank selection.

(b) Noise-aware threshold rank selection.

Figure 2: Monte Carlo success rates for source-number estimation under moment noise. The noise-aware threshold rule is more consistent with the perturbation analysis, while the largest-gap rule is more sensitive for larger source numbers.



(a) Median stability ratio.

(b) Success rate and sufficient-condition rate.

Figure 3: Weyl-type stability diagnostics. The dashed line in panel (a) indicates the sufficient threshold $R = 1/2$. The transition from successful rank recovery to failure occurs when $m\varepsilon_m^{\text{obs}}/\sigma_N(H_m)$ crosses this stability level.

4.3 Resolution limits: close sources and weak sources

The stability theorem shows that reliable numerical rank selection requires

$$m\varepsilon_m < \frac{1}{2}\sigma_N(H_m).$$

Thus the admissible perturbation level is proportional to the smallest nonzero singular value $\sigma_N(H_m)$. We now examine two configurations in which this singular value becomes small: close source locations and weak source strengths.

First, we consider a two-source configuration and decrease the separation $|p_1 - p_2|$. Figure 4(a) plots the smallest signal singular value $\sigma_N(H_m)$ as a function of the source separation. As the two sources approach each other, $\sigma_N(H_m)$ decays rapidly. Although the exact rank remains equal to 2, the numerical rank becomes increasingly difficult to distinguish in noisy data because the admissible perturbation level decreases.

Second, we consider a three-source configuration and gradually decrease the strength q_3 of the third source. Figure 4(b) shows that the smallest signal singular value decreases as the weak source strength is reduced. Therefore weak sources can be missed by numerical rank selection even though they are present in the exact moment sequence.

Figure 5 reports the admissible perturbation level

$$\frac{\sigma_N(H_m)}{2m}$$

predicted by Theorem 3.2. Both close sources and weak sources reduce this admissible level. These results explain the sensitivity observed in the noisy rank experiments: the rank method is stable when the smallest signal singular value is clearly separated from the noise floor, and it becomes unstable when this separation is lost.

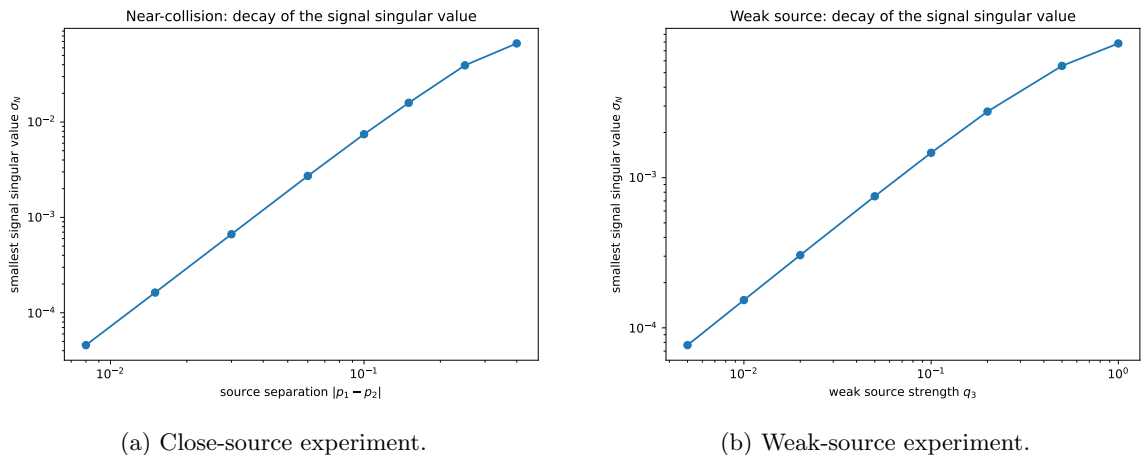


Figure 4: Resolution limits of the moment–Hankel rank method. The smallest signal singular value $\sigma_N(H_m)$ decreases when sources become close or when one source becomes weak.

4.4 Location and strength recovery after rank identification

After the source number has been identified, the same low-frequency moment sequence can be used to recover source locations and strengths. In this experiment, the true value of N is used in the reconstruction step in order to isolate the stability of the Prony–Vandermonde recovery. The locations are obtained from the roots of the annihilating polynomial, and the strengths are then computed by solving the corresponding Vandermonde system.

We measure the location error by

$$E_p = \left(\frac{1}{N} \sum_{j=1}^N |\hat{p}_{\pi(j)} - p_j|^2 \right)^{1/2},$$

where the permutation π is chosen to minimize the matching error. The relative strength error is defined by

$$E_q = \frac{\left(\sum_{j=1}^N |\hat{q}_{\pi(j)} - q_j|^2 \right)^{1/2}}{\left(\sum_{j=1}^N |q_j|^2 \right)^{1/2}}.$$

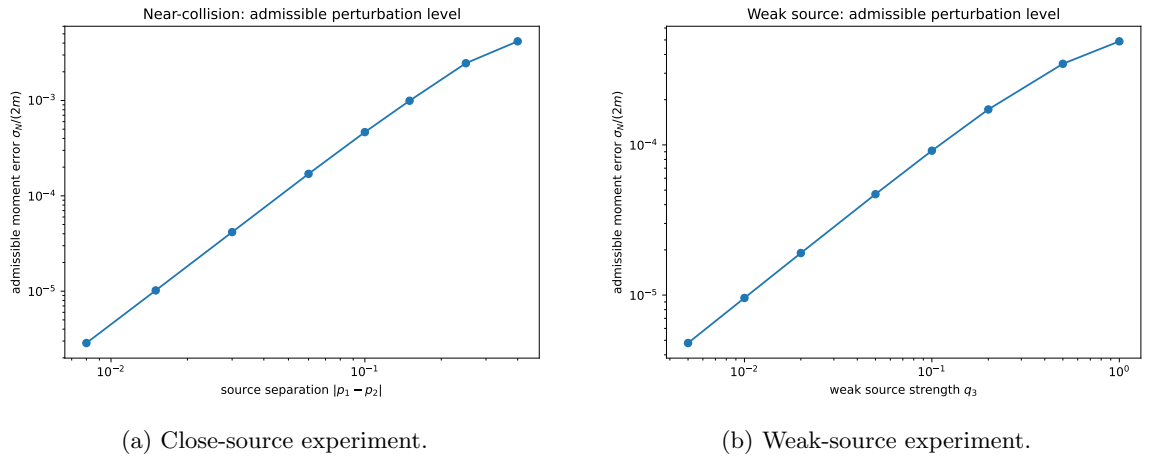


Figure 5: Admissible moment perturbation level $\sigma_N(H_m)/(2m)$ predicted by the stability theorem. Close and weak sources reduce the admissible perturbation level and therefore make numerical rank selection more sensitive to noise.

Figure 6 reports the reconstruction errors for representative source numbers $N = 1, 3, 5$, together with the condition number of the Vandermonde matrix. In all cases, the noiseless reconstruction reaches machine precision. As the moment noise increases, both E_p and E_q increase. The strength error is generally larger than the location error, especially for larger N , because the strengths are recovered from a Vandermonde linear system after the nodes have already been estimated.

The Vandermonde condition number grows rapidly with N . In the tested configurations, it increases from 1 for $N = 1$ to approximately 1.49×10^2 for $N = 5$. This growth explains the deterioration of the reconstruction for larger source numbers. Thus the recovery stage is accurate for small and moderately conditioned configurations, but it becomes sensitive when the Vandermonde system is ill conditioned.

4.5 Summary of the numerical findings

The numerical experiments support the theoretical rank characterization and clarify the practical limitations of the method. In the noiseless case, the Hankel rank exactly recovers the source number once $m \geq N$. Under moment noise, the method remains effective when the stability ratio

$$\frac{m\varepsilon_m^{\text{obs}}}{\sigma_N(H_m)}$$

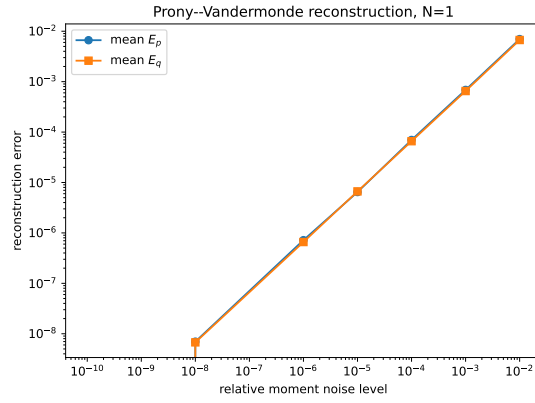
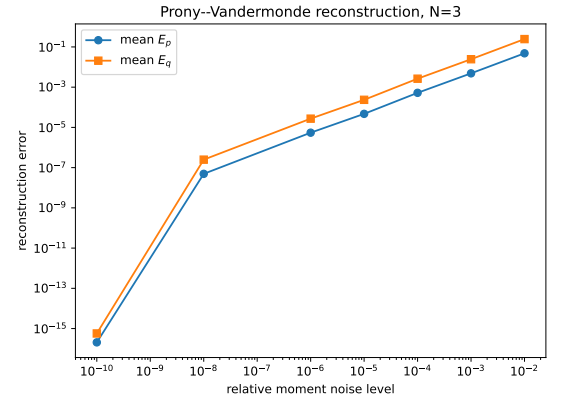
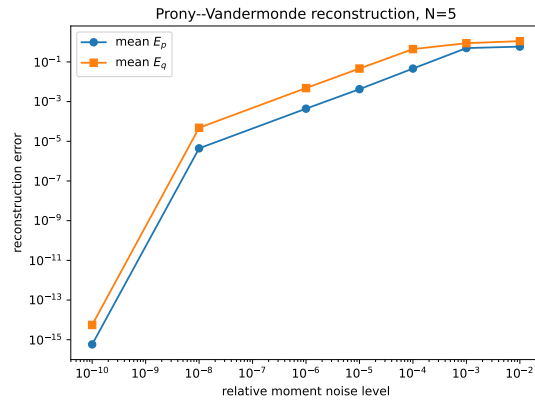
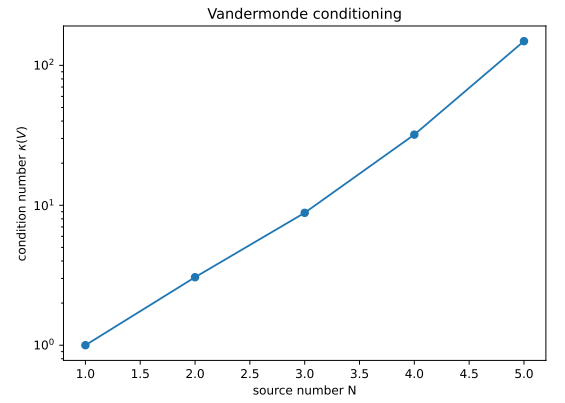
is below the theoretical threshold $1/2$. The main source of failure is rank underestimation, which occurs for larger N , nearly colliding sources, or weak sources. These cases reduce $\sigma_N(H_m)$, thereby reducing the admissible perturbation level predicted by Theorem 3.2.

After the source number is correctly identified, the Prony–Vandermonde step recovers locations and strengths accurately for well-conditioned configurations. The strength recovery is more sensitive than the location recovery because it requires solving a Vandermonde system. Overall, the experiments show that the moment–Hankel rank method is an effective low-frequency source-counting procedure when the significant singular values are separated from the perturbation level.

5 Conclusion

This paper proposed a low-frequency moment–Hankel rank method for identifying the number of stationary point sources in the heat equation in the unit disk. After applying the Laplace transform and normalizing the boundary flux, we considered the low-frequency limit of the resulting boundary data. The positive Fourier moments of this limit were shown to have a finite exponential-sum representation, in which the exponential nodes encode the source locations, the weights encode the source strengths, and the number of exponential terms equals the number of point sources.

The main result shows that the Hankel matrix generated by these moments admits a Vandermonde factorization. Under the natural assumptions that the source locations are distinct and the source strengths are nonzero, the rank of the Hankel matrix is exactly the number of point sources, provided that the Hankel order is no smaller than the true source number. This gives a

(a) $N = 1$.(b) $N = 3$.(c) $N = 5$.

(d) Vandermonde conditioning.

Figure 6: Prony-Vandermonde reconstruction after source-number identification. The reconstruction is accurate for small N and small moment noise, but deteriorates as N increases because the associated Vandermonde system becomes more ill conditioned.

direct deterministic source-counting principle based on the low-frequency moment sequence. Compared with determinant zero-counting methods in the complex Laplace-frequency plane, the present approach avoids contour integration and reduces the counting step to a finite-dimensional numerical rank problem.

We also discussed the implementation of the rank criterion from discrete and noisy boundary data. In practical computation, the exact Hankel rank is replaced by the numerical rank determined from the singular values of the empirical Hankel matrix. The numerical experiments confirm the theoretical rank pattern in the noiseless case and show that the method can reliably identify the source number when the significant singular values are well separated from the noise floor. The experiments further demonstrate that close sources and weak sources reduce the smallest signal singular value, thereby making the numerical rank selection more sensitive to noise.

After the source number is identified, the same moment sequence can be used to recover source locations and strengths through an annihilating-polynomial and Vandermonde reconstruction procedure. The numerical results show accurate recovery for well-conditioned configurations, while also indicating that the strength reconstruction is more sensitive than the location reconstruction due to the conditioning of the Vandermonde system.

The present work focuses on the unit disk, where the low-frequency Fourier moment representation is explicit. Extensions to more general domains, development of more robust numerical rank-selection rules, and regularized moment reconstruction under stronger noise are natural directions for future work.

References

- [1] B. Abdelaziz, A. El Badia, and A. El Hajj. Direct algorithms for solving some inverse source problems in 2d elliptic equations. *Inverse Problems*, 31(105002):26pp, 2015.
- [2] A. E. Badia, T. H. Duong, and A. Hamdi. Identification of a point source in a linear advection-dispersion-reaction equation: Application to a pollution source problem. *Inverse Problems*, 21:1121–1136, 2005.
- [3] S. Baillet, J. C. Mosher, and R. M. Leahy. Electromagnetic brain mapping. *IEEE Signal Processing Magazine*, 18(6):14–30, 2001.
- [4] L. Baratchart, A. B. Abda, F. B. Hassen, and J. Leblond. Recovery of pointwise sources or small inclusions in 2d domains and rational approximation. *Inverse Problems*, 21:51–74, 2005.
- [5] I. Bushuyev. Global uniqueness for inverse parabolic problems with final observation. *Inverse Problems*, 11(L11-L16), 1995.
- [6] J. R. Cannon and P. DuChateau. Structural identification of an unknown source term in a heat equation. *Inverse Problems*, 14(3):535, 1998.
- [7] M. Choulli. An inverse problem for a semilinear parabolic equation. *Inverse Problems*, 10:1123–1132, 1994.
- [8] Z. Deng, A. Qian, and X. Yang. A Hankel determinant zero-order principle for source counting in an inverse heat point-source problem. <https://arxiv.org/abs/2606.15065>.
- [9] Z. L. Deng, C. Li, and X. M. Yang. A Bayesian thinning algorithm for the point source identification of heat equation. <https://arxiv.org/abs/2509.14245>, 2025.
- [10] A. Gallet, S. Rigby, T. N. Tallman, X. Kong, I. Hajirasouliha, A. Liew, D. Liu, L. Chen, A. Hauptmann, and D. Smyl. Structural engineering from an inverse problems perspective. *Proceedings of Royal Society A*, 478(20210526), 2022.
- [11] F. Gong, B. Jin, Y. Kian, and S. Liu. Identification of a point source in the heat equation from sparse boundary measurements. *arXiv preprint*, 2026.
- [12] Q. Gu, W. Zhang, and Z. Zhang. Determine the point source of the heat equation with sparse boundary measurements. *SIAM Journal on Applied Mathematics*, 85(5):2337–2354, 2025.
- [13] B. He, A. Sohrabpour, E. Brown, and Z. Liu. Electrophysiological source imaging: A noninvasive window to brain dynamics. *Annual review of biomedical engineering*, 20:171–196, 2018.
- [14] V. Isakov. *Inverse Source Problems*. American Mathematical Society, Providence, RI, 1990.

- [15] V. Isakov. Inverse parabolic problems with the final overdetermination. *Communications on Pure and Applied Mathematics*, 44(2):185–209, 1991.
- [16] Y. Kian and M. Yamamoto. Reconstruction and stable recovery of source terms and coefficients appearing in diffusion equations. *Inverse Problems*, 35(11), 2019.
- [17] V. Komornik and M. Yamamoto. Upper and lower estimates in determining point sources in a wave equation. *Inverse Problems*, 18:319–329, 2002.
- [18] I. V. Kovalets, S. Andronopoulos, A. G. Venetsanos, and J. G. Bartzis. Identification of strength and location of stationary point source of atmospheric pollutant in urban conditions using computational fluid dynamics model. *Mathematics and Computers in Simulation*, 82:244–257, 2011.
- [19] L. Ling, M. Yamamoto, Y. C. Hon, and T. Takeuchi. Identification of source locations in two-dimensional heat equations. *Inverse Problems*, 22(4):1289, 2006.
- [20] A. V. Mamonov and Y-H R. Tsai. Point source identification in nonlinear advection diffusion reaction systems. *Inverse Problems*, 29(035009), 2013.
- [21] M. B. Moghaddam, M. Mazaheri, and J. M. V. Samani. Inverse modeling of contaminant transport for pollution source identification in surface and groundwaters: a review. *Groundwater for sustainable development*, 15(100651), 2021.
- [22] T. Ohe, H. Inui H, and K. Ohnaka. Real-time reconstruction of time-varying point sources in a three-dimensional scalar wave equation. *Inverse Problems*, 27(115011), 2011.
- [23] D. E. Reeve and M. Spivack. Determination of a source term in the linear diffusion equation. *Inverse Problems*, 10:1335–1344, 1994.
- [24] K. Ren and Y. Zhong. Imaging point sources in heterogeneous environments. *Inverse Problems*, 35:125003, 2019.
- [25] W. Rundell and D. L. Colton. Determination of an unknown non-homogeneous term in a linear partial differential equation from overspecified boundary data. *Applicable Analysis*, 10(3):231–242, 1980.
- [26] S. Shlomi and A. M. Michalak. A geostatistical framework for incorporating transport information in estimating the distribution of a groundwater contaminant plume. *Water resources research*, 43(W03412), 2007.
- [27] V. V. Solov'ev. On the solvability of the inverse problem of determining a source with overdetermination on the upper base for the parabolic equation. *Differential Equations*, 25:1114–1119, 1989.
- [28] S. Vessella. Locations and strengths of point sources: stability estimates. *Inverse Problems*, 8(911–917), 1992.